Nanoscale

Accepted Manuscript

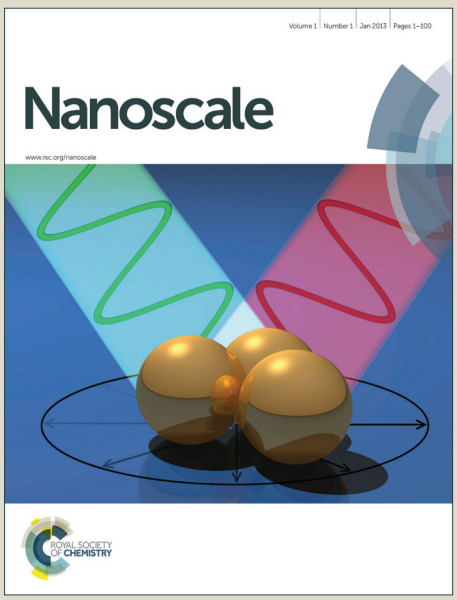

ROYAL SOCIETY OF CHEMISTRY

www.rsc.org/nanoscale

Nanoscale

RSCPublishing

PAPER

One-step synthesis of graphene/polyaniline hybrids by *in situ* intercalation polymerization and their electromagnetic properties

Xiangnan Chen,[a] Fanchen Meng,[a] Zuowan Zhou,*[a] Xin Tian,[a] Liming Shan,[a] Shibu Zhu,[a] Xiaoling Xu,[a] Man Jiang,*[a] Li Wang,[b] David Hui,[c] Yong Wang, *[a] Jun Lu[a] and Jihua Gou[d]

Cite this: DOI: 10.1039/x0xx00000x

Received 00th January 2012,
Accepted 00th January 2012

DOI: 10.1039/x0xx00000x

www.rsc.org/

A new method is introduced on preparation of graphene/polyaniline hybrids using a one-step intercalation polymerization of aniline in-site the expanded graphite. The structural and morphological characterizations were performed by X-ray diffraction analysis, transmission electron microscopy and field emission scanning electron microscopy. Both experimental and first-principles simulated results show that aniline cation formed by aniline and H^+ tends to be drawn towards the electron-enriched zone and to intercalate into the interlayer of graphite. Subsequently, an *in situ* polymerization leads to the graphite's separating into graphene sheet resulting from the exothermic effect and more vigorous movements of the chain molecules of polyaniline. The interactions between polyaniline and graphene were confirmed by Fourier transformed infrared spectroscopy as well as Raman spectra. Besides, the graphene/polyaniline hybrid exhibited a breakthrough in improvement of microwave absorption.

[a] Key Laboratory of Advanced Technologies of Materials (Ministry of Education), School of Materials Science and Engineering, Southwest Jiaotong University, Chengdu 610031, China. Fax, Tel: +86 028-87600454. E-mail: zwzhou@at-c.net (Z. Zhou), jiangman1021@163.com (M. Jiang).

[b] China Academy of Space Technology, Beijing 100094, China

[c] Department of Mechanical Engineering, University of New Orleans, New Orleans, LA 70148, United States

[d] Department of Mechanical, Materials and Aerospace Engineering, University of Central Florida, Orlando, FL 32816, United States

Nanoscale RSCPublishing

PAPER

Introduction

Graphene, two dimensional layers of sp^2-bonded carbon, has recently become the object of numerous investigations because of its potentially interesting applications in transistors,[1] hydrogen storage materials,[2] sensors,[3] microwave absorbing materials[4] and some other fields.[5] The Nobel Prize in Physics in 2010 was awarded jointly to Andre Geim and Konstantin Novoselov for their ground-breaking works regarding the two-dimensional material graphene.[6] Since then, various methods of preparing graphene have been explored, such as mechanical cleavage,[7] liquid-phase exfoliation of graphite,[8] and chemical reduction of graphene oxide,[9] epitaxial growth on SiC,[10] and chemical vapor deposition (CVD).[11] It is obvious that within these techniques exist limitations or shortcomings. The mechanical methods always have great demanding on experimental equipments and/or operation procedures, while the chemical methods using super acid or strong oxidize agent causes harm to experimental facilities and environmental pollution. In short, safely mass production of graphene has so far been very limited. So, it is of great importance to develop an environmentally-friendly method for the preparation of graphene.

To date, efforts have also been made for preparation of graphene-contained composites, such as graphene/polyaniline (PANi) hybrids for new functional applications.[12-15] The widely used method for preparing graphene/PANi hybrids or composites is chemical reduction of graphite oxide pre-prepared by Hummers method which actually involves the use of super acid or strong oxidizing agent.[16]

The key problem to separate the graphite sheets is to overcome or destroy the strong van der Waals-like forces between layers of graphite. Some works have focus on the ultrasound-assisted method for preparation of graphene using dispersing agents or additives, such as supercritical CO_2,[17] supercritical N, N dimethylformamide,[18] and Gum Arabic.[19] Another new method for preparation of graphene is to use intercalating agents such as K^+ and other metal cations,[20] and there exist huge cation-π interactions between the metal cations and graphene.[21,22] It appears that the PANi may intercalate into the graphite oxide as an incidental phenomenon, but no experimental data has been reported, let alone explanation or mechanism.[23,24] When pH of the solution is lower than 4, aniline cation (ANi^+) could be formed by aniline (ANi) and H^+.[25] So it is of great possibility to use the intercalation polymerization of ANi^+ overcoming the van der Waals-like forces between the graphite layers and finally obtained graphene hybrid structure. Besides, the expanded graphite (EG) has much larger inter-planar spacing which can be easier to be intercalated.

In the present paper, we report a new approach of one-step method for preparing graphene/PANi hybrids by an *in situ* polymerization of ANi intercalating into the EG and have investigated the formation mechanism of the hybrids. The as-synthesized hybrid shows a significantly enhancement in microwave absorption.

Results and discussion

Morphology and Structure of the Nanocomposites

The morphologies of the used EG, EG mixed with ANi^+ (denoted as ANi^+/EG) and the hybrid were characterized by FE-SEM and TEM observations. As shown in Fig. 1 a, the EG we used in this work was a kind of typical wormlike multilayer graphite structures. For ANi^+/EG sample (Fig.1 b), it was obvious that after dispersion, in the presence of the ANi^+, the EG displayed a better dispersity. This indicated that the ANi^+ have separated the graphite layers in some extent. From Fig.1 c, showing the TEM image of the as-prepared PANi/EG-1, it could be clearly recognized the ribbon-like PANi nanofibers and large-scaled few layer graphene (as marked by arrows). This demonstrated that the *in-situ* polymerization made a further separation of the graphite.

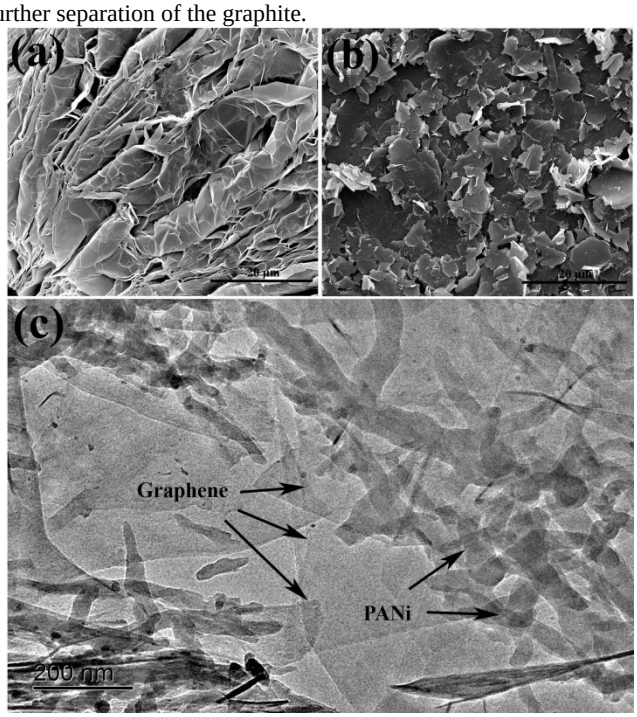

Fig. 1 FE-SEM images of (a) EG (b) EG mixed with ANi^+ and TEM image of (c) the composites obtained by intercalation polymerization of ANi^+ into 1 wt % EG (denoted as PANi/EG-1).

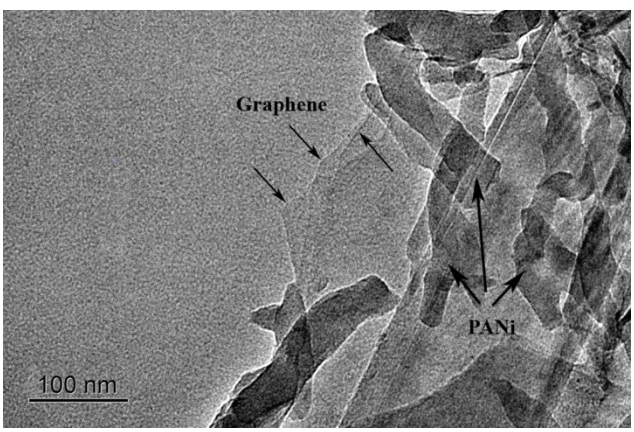

Fig. 2 TEM image of PANi/EG-1.

A more meticulous TEM image of the PANi/EG-1 was shown in Fig. 2. Arrows have been marked in the picture to point out the existence of few layer graphene. Ribbon like PANi nanofibers were also found to have been successfully intercalated into the graphene. From the above analysis, it is convinced that the graphene hybrids have been synthesized through the *in situ* intercalation polymerization of ANi^+ into the EG.

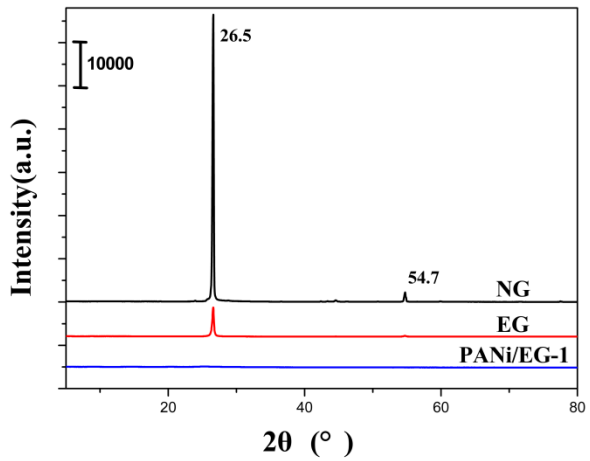

Fig. 3 XRD patterns of natural graphite (NG), EG and PANi/EG-1.

In Fig. 3 it was depicted that the XRD patterns of natural graphite (NG) and EG both exhibited sharp characteristic diffraction peak at 2θ = 26.5° (d=3.369 Å), which was assigned to (002) plane of graphite.[26] Normally when graphite was expanded, the diffraction peak of graphite (002) plane became broad or smaller. These phenomena were owning to the disorganization on c axis. The decrease of the relative intensity of this peak for EG was due to the disorganization on c axis of EG which was agreed with the results of SEM observation (Fig. 1 a). However, this diffraction peak seemed rapidly diminishing for PANi/EG-1, confirming a severely disorganization on c axis and the graphite having been separated into mono or few-layered sheets after intercalation polymerization of ANi^+ into the interlayer of EG. And this also agreed to the TEM image of PANi/EG-1(Fig. 2).

Further evidence was given in Fig. 4, which gave the XRD patterns of the grinding mixture of PANi and 1 wt % EG (PANi/EG-0) and graphene/PANi hybrids (PANi/EG-1). In addition to the diffraction peaks of PANi (2θ = 8.9, 14.8, 20.4, 25.3°),[27] the XRD pattern of PANi/EG-0 displayed a sharp diffraction peak at 2θ = 26.5° and a small peak at 54.7°, representing graphite (002) and (004) plane, respectively, which illustrated a distinguishing comparison with the XRD pattern of PANi/EG-1, synthesized through an intercalation polymerization of ANi in-site the EG. It further proved that the sharp decrease of the relative intensity of the diffraction peak at 2θ = 26.5° was due to the separation of the graphite layers caused by the in situ intercalation polymerization of ANi^+ rather than the low content of graphite. However, the broad peak at around 2θ=25° (d=3.554 Å) was believed to be the characteristic peak of graphene (002) plane[24, 28] overlapping with the peak of PANi (200) plane. Besides, one could see the characteristic diffraction peak at 2θ = 25° changed a lot in PANi/EG-1 as compared to PANi/EG-0, which further demonstrated the intercalating of PANi into graphene. The broadening and shifting up of the graphene (002) plane was attributed to the increased disorganization on the c axis in graphene[29] caused by the intercalation of PANi.

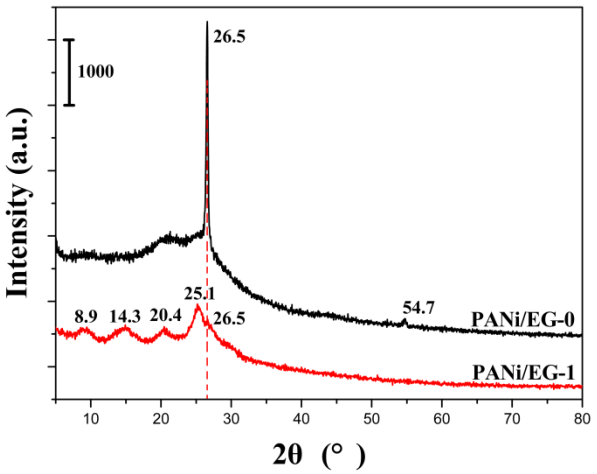

Fig. 4 XRD patterns of the grinding mixture of PANi and 1 wt % EG (PANi/EG-0) and graphene/PANi hybrids (PANi/EG-1).

Further Analyses of the *in situ* Intercalation Polymerization

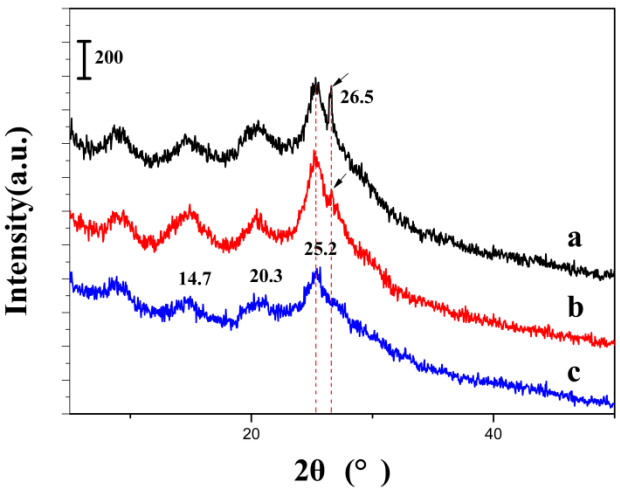

Fig. 5 XRD patterns of (a) product obtained through intercalation polymerization of ANi into 1 wt % EG, mixing the ANi and EG without any solvent and adding HCl aqueous solution after the mechanical stirring and sonication (PANi/EG-2); (b) graphene/PANi hybrids (PANi/EG-1) and (c) HCl doped PANi (HCl-PANi).

When ANi was added into the HCl solution, ANi^+ would be formed by ANi and H^+ that played a key role for intercalating. This is confirmed by changing the order of adding HCl solution during the experiments. The sample of PANi/EG-2 was obtained by mixing 1 wt % EG into ANi firstly, then adding APS in HCl aqueous solution, and followed the same procedures of polymerization. As shown in Fig. 5, the XRD patterns of each sample displayed a characteristic peak at 2θ = 25.2° that is associated with the PANi molecular orientation. A low intensity peak appeared in the composites (Fig. 5 a, b) at around 2θ = 26.5° corresponding to (002) planes of graphite. It was obvious that the PANi/EG-1 exhibited a very weak peak at 2θ = 26.5° corresponding to graphite (002) plane, while PANi/EG-2 displayed a sharp one. For PANi/EG-2, HCl was added only in the second procedure and could not form ANi^+ firstly. So, the ANi^+ was the critical species of intercalation rather than ANi itself. This was a further demonstration that for the PANi/EG-1, the graphite had been

separated into graphene and formed graphene/PANi hybrids during the *in situ* polymerization.

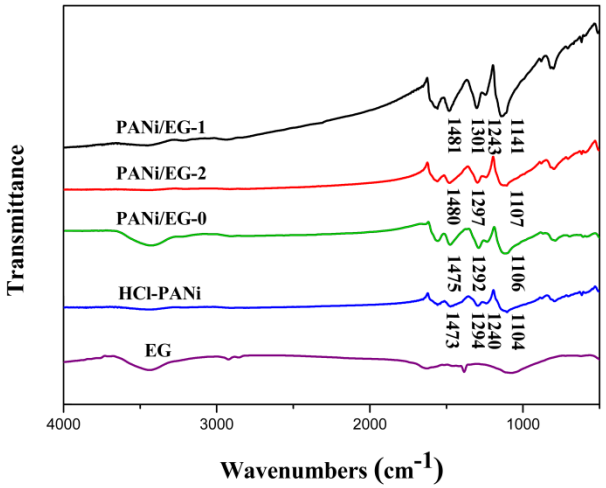

Fig. 6 FTIR spectra of PANi/EG-1, PANi/EG-2 , PANi/EG-0, EG and HCl-PANi.

FTIR was used to analyze the interaction between the PANi and graphene (Fig. 6). The FTIR spectra of PANi/EG-0, EG, HCl-PANi were also provided for comparison. The FTIR spectrum of PANi/EG-0 was found to be almost the same as that of HCl-PANi, which indicated that no significant interactions existed between PANi and EG in PANi/EG-0. While, for both PANi/EG-1 and PANi/EG-2, vibrational bands at about 1473 cm^{-1} were due to the C=C stretching vibrations of the benzene rings, and the bands at about 1294 cm^{-1} could be attributed to the C-N-C stretching.[30] The blue shifts of these two vibrations as compared with those of HCl-PANi (to 1480 and 1297 cm^{-1} in PANi/EG-1, to 1481 and 1301 cm^{-1} in PANi/EG-2) might be ascribed to the π-π interactions between the PANi molecules and the graphene, which hindered the movements of the associated groups. One could see that C-N-C stretching vibrations of the Quinone imine at 1240 cm^{-1} in PANi[31] displayed a blue shift to 1243 cm^{-1} in PANi/EG-1, while it did not occur in PANi/EG-2. Besides, the bands at about 1104 cm^{-1} due to the Q=N stretching vibrations (where Q represented the quionoid ring) exhibited a blue shift of 37 cm^{-1} in PANi/EG-1. All these phenomena demonstrated that in the composites there existed hybridizing interactions between the N-atom in PANi and π-electrons in graphene. Besides, PANi/EG-1 displaying greater blue shifts demonstrated that ANi^+ was more favourable to give an intercalation polymerization into EG. This may be due to the π-π interactions and electron donor and acceptor interactions between ANi^+ and the π-electrons in EG.

In conjunction with FTIR spectroscopy, the formation of PANi/graphene hybrids has also been confirmed by Raman scattering (Fig. 7). The characteristic bands of PANi, such as 1164 cm^{-1} band attributing to the in plane C-H bending of Quinoid units, 1342 cm^{-1} band assigning to C-N+• stretching, 1474 cm^{-1} band being due to N=C=N stretching of the Quinoid di-imine units and the band at 1590 cm^{-1} representing C=C stretching of the Quinoid units,[32] could be obviously observed in Raman spectroscopy of HCl-PANi. The Raman spectrum of EG showed the typical D band (1350 cm^{-1}) attributing to the defects and edge areas, G band (1580 cm^{-1}) corresponding to the vibration of the sp^2-hybridized carbon and 2D band (2710 cm^{-1}) due to the double resonant scattering process from zone-edge phonons.[33] The typical D-band, 2D-band and the characteristic bands of PANi could also be observed in the spectrum of PANi/EG-0 with almost no shift and change, which further proved that there existed no intercalating or hybridizing interactions in PANi/EG-0. Interestingly, all these bands disappeared in the Raman spectrum of PANi/EG-1 while two new broad bands at 1352 and 1575 cm^{-1} appeared. These two bands were agreed with the D-band and G-band of graphene, but not as sharp as those two bands, respectively.[34] The high intensity of the D-band as well as the overlapping of the D-band and G-band indicated that the introduction of N-atom brought out much more defects and disordered structure into the graphene. The broad and overlapped peaks suggested that the system was highly disorganized. The presence of G band with this profile could be assigned to the presence of small clusters of graphite. However, the loss of the 2D band in the PANi/EG-1 further suggested that the clusters of graphite should be composed of few layer graphene.[35] Overall, for the graphene/PANi hybrids, there existed strong interactions between the N-atoms in PANi and the π-electrons in graphene. Further more, the interactions and the overlapping of the 2p orbit of N-atoms and p orbit of graphene affected the large π-system in graphene.

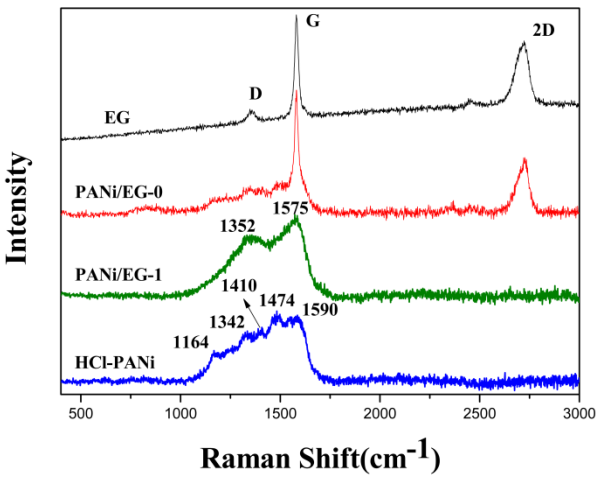

Fig. 7 Raman spectra of PANi/EG-1, PANi/EG-0, EG and HCl-PANi.

First-principles Study of ANi^+ Intercalated Bilayer Graphene

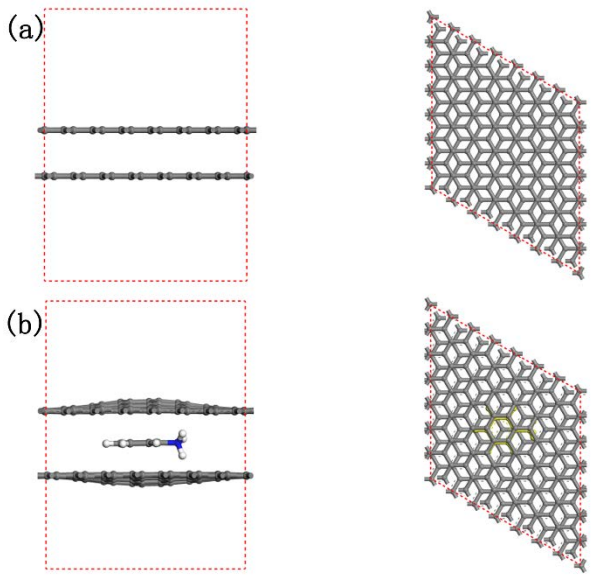

Fig. 8 Geometric structures of a. bilayer graphene and b. ANi^+ intercalated bilayer graphene. The unit cell is enclosed by red dashed rectangle.

Combined with the above experimental results, we have also done some further simulation. In order to theoretically verify the experimental results and explore the intercalation mechanism, it is necessary to do a calculation based on Density Functional Theory (DFT). Actually, the ideal bilayer graphene system could provide adequate information of the intercalation process. DFT calculation was carried out to investigate the formation energy (E_{form}) of ANi^+ intercalated bilayer graphene. Generalized gradient approximation (GGA) of Perdew, Burke and Ernzerhof,[36,37] as implemented in the DMol3 package,[38] was employed in the calculation. A 7×7 super cell of bilayer graphene (17.22 Å along a and b directions), which was large enough to avoid the image interaction of ANi^+, was used in the simulation. The calculation was treated with the slab model, in which the neighbouring surfaces are separated by 20 Å of vacuum. The Brillouin zone is sampled by a $3 \times 3 \times 1$ k-point grid.[39] Theoretical calculations were performed by using dispersion-corrected density functional theory (DFT-D) provided by the DMol3 code. We used the standard parameter set of Grimme without optimization.[40] The calculated distance between the two layers of bilayer graphene was 3.374 Å, which agreed well with the experimental value (d=3.369 Å) calculated from the XRD data of NG. The geometric structures and the chosen unit cell of bilayer graphene and ANi^+ intercalated bilayer graphene are shown in Fig. 8.

The formation energy of optimized structures is given by:

$$E_{form} = 2 \times E(monolayer) + E(ANi^+) - E(ANi^+@bilayer) \quad (1)$$

where E(monolayer) is the total energy of a monolayer graphene; $E(ANi^+)$ is the energy of ANi^+ at its equilibrium structure; $E(ANi^+@bilayer)$ donates the total energy of the complex.

According to Equation (1), the calculated formation energy of ANi^+ intercalated bilayer graphene is 2.81 eV. The positive value indicates an energetically favorable reaction. In the calculation, we used different parameters contributing to the experimental results difference, namely, the charge difference. We have set the total charge of ANi^+ to be 1, and the charge of ANi to be 0. It is interesting to note that the calculated formation energy of ANi intercalated bilayer graphene is 2.01 eV. Though it is also an energetically favorable reaction, the value is smaller than that of ANi^+ intercalated bilayer graphene, which could help to explain why ANi^+ is more favorable to intercalate into the EG than ANi itself. And this is agree with experimental results.

Mechanism for the Formation of Graphene/PANi Hybrids

Based on the above experimental and simulation results, a possible mechanism for the formation of graphene/PANi hybrids by this one-step method was illustrated in Fig. 9. After adding ANi into the mixed suspension of HCl and EG, the ANi^+ would be formed first (Fig. 9 I). This cationic complex would squint toward the electron-enriched zone, the conjugated π-electrons between the layers of graphite (Fig. 9 II). This could also be explained by the electron donor and acceptor interactions between the π-electron system in EG and the ANi^+. As more cationic complexes formed and inserted into the layers, the intercalated ANi^+ made the graphite turn to larger spaces and accordingly weaken the interactions between the interlaminations. When the oxidant and initiator APS was added, an *in situ* polymerization would take place onsite, leading to macromolecules formation and a large amount of heat generation.[41] The movements of the long chain molecules of PANi and the exothermal effect led to a violent separation of graphite into graphene that was pasted and stabled by the onsite synthesized PANi molecule (Fig. 9 III).

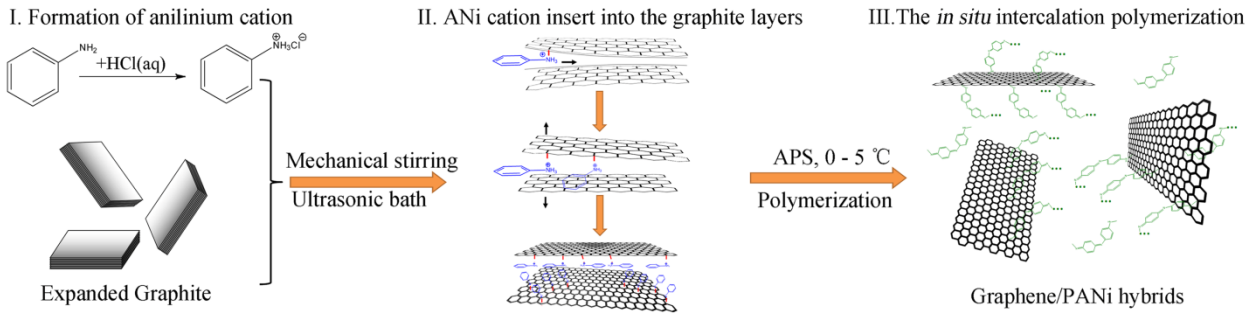

Fig. 9 Schematic for intercalation polymerization of ANi^+ into EG to synthesize graphene/PANi hybrids.

Conductivity of the Graphene/PANi Hybrids

Table 1 The conductivities of the related samples

Sample No.	Sample Name	Conductivity (S/cm)
1	HCl-PANi	1.47
2	PANi/EG-0	3.50
3	PANi/EG-1	0.47
4	PANi/EG-2	1.33
5	EG	262.74

The samples were all pressed into circular sheet (thickness = 0.5 mm, diameter = 1 cm). The values of conductivity by a four-probe measurement of the related samples were listed in Table 1. For PANi/EG-0, 1 wt % EG's introduction made an increase of conductivity from 1.47 to 3.50 S/cm, being due to the high conductivity of EG (262.74 S/cm). However, for the as-prepared hybrids, the conductivity displayed obvious deceases as compared to those of HCl-PANi or the graphene. The latter showed more evidently decrease of the conductivity. This was mainly caused by the hybridizing interactions between the PANi and the graphene. According to the discussions of the XRD, FTIR and Raman data, it has been proved that there exist hybridizing interactions between the PANi and graphene. It was also believed that the hybridizing interactions brought about more defects and disordered part, which sharply decreased the conductivities of graphene.[42] Firstly, the formation of the hybrids of PANi and graphene reduced the doping

degree of PANi, resulting in a lower carrier concentration. Secondly, the interaction between the N-atoms on PANi molecular chain and the π-electron on graphene plane affected or destroyed the large conjugated system in graphene, leading to influencing the charge transfer in PANi and destroying the conjugated π-system in graphene both alone. Additionally, there also might exist π-π staking in the graphene/PANi hybrids.[43] Thus, the conductivity of the hybrids of PANi and graphene displayed unconventional decrease as compared to those of the HCl doped PANi or the EG.

Electromagnetic Properties of Graphene/PANi Hybrids

According to the transmission line theory, the reflection loss (RL) of the electromagnetic (EM) wave could be calculated from the measured complex permeability and permittivity data by using the following equations: [44]

$$RL = 20 \log \left| \frac{(Z_{in} - Z_0)}{(Z_{in} + Z_0)} \right|, \quad (2)$$

$$Z_{in} = Z_0 \sqrt{\mu_r / \varepsilon_r} \tanh[j(2\pi f d / c \sqrt{\varepsilon_r \mu_r}], \quad (3)$$

where Z_{in} is the input characteristic impedance at the absorbing material/free space interface, Z_0 is the impedance of free space. The μ_r and ε_r are the measured relative complex permittivity and permeability of the material, respectively. d is the thickness of the microwave absorbing material, and c and f are the velocity of light and the frequency of microwave in free space, respectively.

Based on the electromagnetic parameters (the complex values of permeability and permittivity), the RL could then be calculated for the given frequency with various thicknesses according to Equation (2) and (3). Fig. 10 give the calculated RL results of the five materials for assumed thickness of 3.5 mm. As one can see, EG, PANi, PANi/EG-0 and even PANi/EG-2 displayed poor microwave absorption performance. Surprisingly, the obtained hybrid PANi/EG-1 showed a breakthrough in improvement of microwave absorption. With a thickness of 3.5 mm, the optimal absorption peak reached -36.9 dB at 10.3 GHz and the bandwidth corresponding to the reflection loss at -10 dB was 5.3 GHz (from 8.2 to 13.5 GHz).

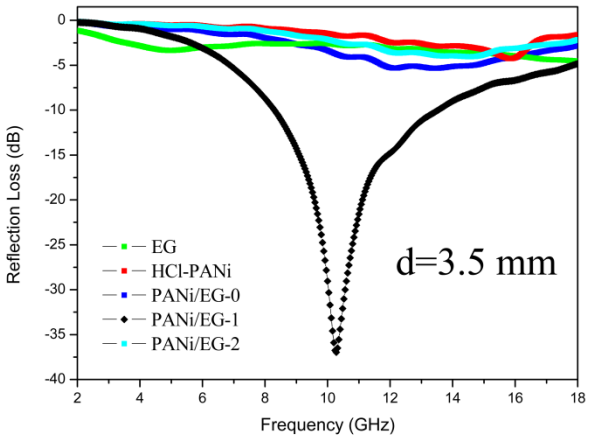

Fig. 10 Calculated RL of the samples with a thickness of 3.5 mm in the frequency range of 2-18 GHz.

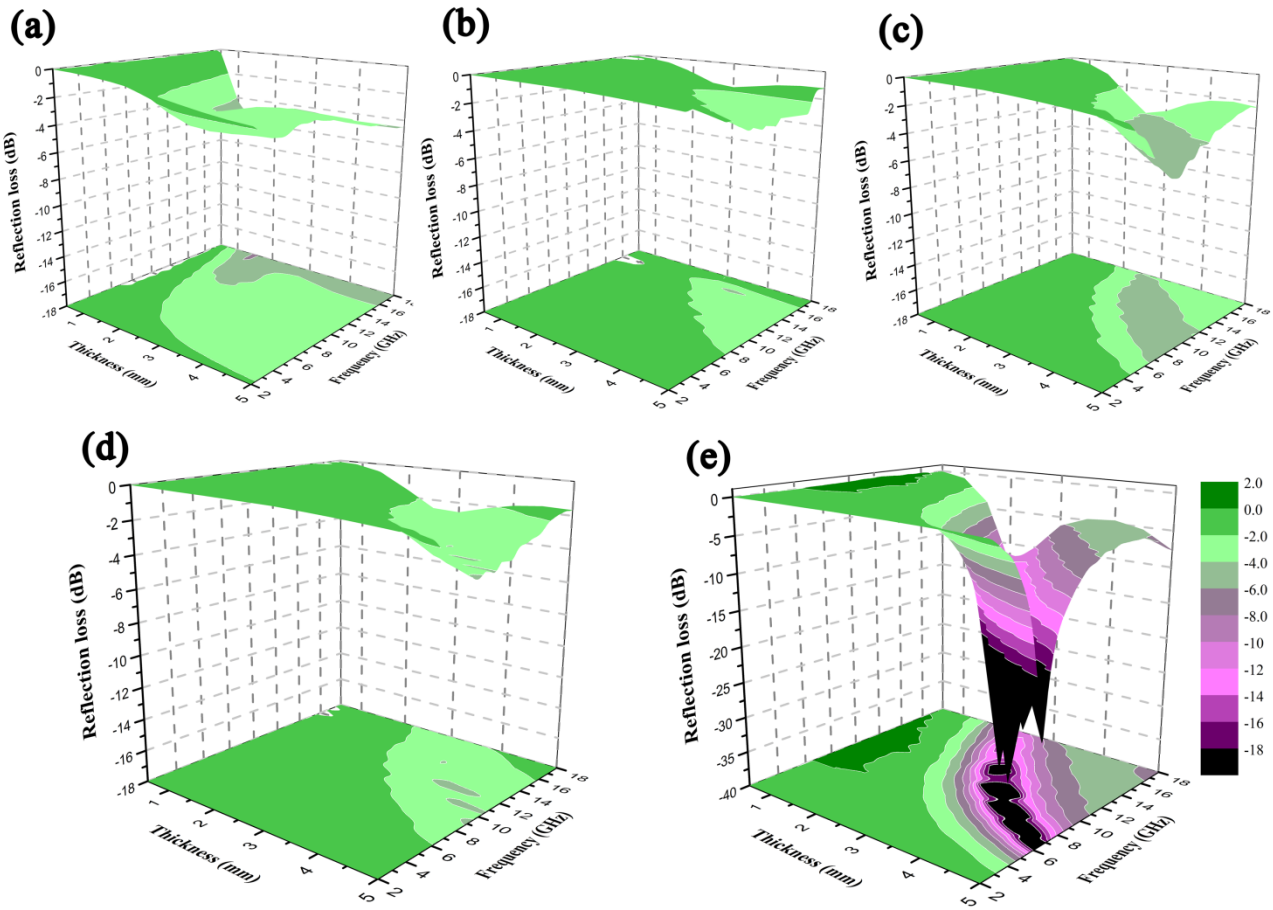

Fig. 11 Three-dimensional representations of RL of (a) EG, (b) PANi, (c) PANi/EG-0, (d) PANi/EG-2, (e) PANi/EG-1.

We also simulated the microwave losses of the five materials with different thickness. Fig. 11 displayed visual three-dimensional maps for helping us to compare the microwave absorption properties of the five materials. The minimum RL reached -36.9 dB with a thickness of 3.5 mm for PANi/EG-1, while the other four kind of materials displayed almost no RL. Moreover, it could be observed that the absorption bandwidth with RL below -10 dB was obtained in the frequency range of 5-18 GHz for PANi/EG-1 with a thickness of 2.3-5 mm. It was obvious that PANi/EG-1 exhibited the most superior performance to other samples in microwave absorption with a higher microwave loss and a wider absorption bandwidth (Fig. 11 e).

The complex permittivity real part (ε'), permittivity imaginary part (ε"), permeability real part (μ'), and permeability imaginary part (μ") of EG, PANi, PANi/EG-0, PANi/EG-1 and PANi/EG-2 were investigated in the frequency of 2-18 GHz (Fig. S1). The effective regulation of resistance could affect the corresponding real and imaginary parts of complex permittivity, For PANi/EG-1, the decrease of the conductivities might lead to the balance of dielectric loss and magnetic loss, inducing better impedance match and superior EM wave absorption. [45]

The improved microwave absorption of PANi/EG-1 might be attributed to the better impedance match. And what was more, it was also believed that the special hybridizing structure of graphene and PANi brought out new mechanisms for microwave absorption. For the graphene/PANi hybrids, there existed strong interactions between the N-atoms in PANi and the π-electrons in graphene, and the large conjugated system in graphene was also destroyed. So it would generated more defects and hybridizing points, acting as new centers of polarization and causing additional relaxation, and accordingly leading to energy dissipating by interacting with the incident microwave. [4] Besides, The special lamellar and interfacial structure of the graphene/PANi hybrids might also bring about an expanded propagation path of EM wave through the multiple reflections. [46]

Experimental details

Materials

Expandable graphite (325 mesh, H_2O < 1.0%) was purchased from Qingdao KangBoEr Graphite Products Co., Ltd. (China). Before it was used, the expandable graphite was calcinated (Muffle furnace, 900 ℃,30 s) to obtain EG. ANi was distilled under reduced pressure (35 mmHg, 85 ℃) and stored below 0 ℃. Other chemicals, such as ammonium peroxydisulfate (APS, $(NH_4)_2S_2O_8$), 36% hydrochloric acid (HCl) were analytical grade, and were used as received without further purification. All experiments were carried out using deionized water.

Preparation of HCl Doped PANi and PANi/EG Grinding Mixture

The synthesis of PANi doped with HCl by *in situ* polymerization was conducted in aqueous solution with APS as oxidant through a typical process below, 2 mmol of ANi (0.2 ml) and 20 ml 1 N HCl aqueous solution was mixed. Before polymerization, the mixture was cooled in an ice bath (ca. 0-5 ℃) and stirred for 30 min. Then 1.6 mmol of APS dissolved in 10 ml 1 N HCl aqueous solution was slowly added into the above cooled solution, and the resulting solution was mechanically stirred for about 2 min. The mixture was kept for polymerization at 0-5 ℃ for 16 hours (h). The resulting dark green precipitate was washed with deionized water and ethanol for three times, and was dried in vacuum oven at 60 ℃ for 24 h. And finally, the HCl doped PANi was obtained (denoted as HCl-PANi). Then 1 wt % EG to ANi was added into the HCl-PANi powder. The mixture was grinded in an agate mortar for 10 min to obtain the HCl-PANi/EG grinding mixture (denoted as PANi/EG-0).

Preparation of Graphene/PANi Hybrids

2 mmol of ANi (0.2 ml) and 20 ml 1 N HCl aqueous solution was mixed, and the mixture was cooled in an ice bath (ca. 0-5 ℃) and stirred for 30 min to obtain ANi^+. Then 1 wt % EG was added into the above cooled solution. The solution was further carried on a mechanical stirring (300 rpm) for 4 h under ice bath. Then the obtained mixture was given a mild sonication (40 KHz, ultrasonic bath) for 1 h. 1.6 mmol of APS dissolved in 10 ml 1 N HCl aqueous solution was then slowly added into the above cooled solution with a slow stirring. The mixture was kept for polymerization at 0-5 ℃ for 16 h. The resulting dark green precipitate was washed with deionized water and ethanol for three times, and was dried in a freeze-drying system. Finally, the powder was gathered as the product (denoted as PANi/EG-1).

Comparatively, 20 ml ANi and 1 wt % EG (0.186 g) was mixed without any solvent under ice bath (0-5 ℃). The mixture was given the same dispersion process as the preparation of PANi/EG-1. Then, 0.2 ml of the above cooled mixture and 20 ml 1 N HCl aqueous solution was then mixed. The mixture was then carried on the same polymerization process as PANi/EG-1. This product was called PANi/EG-2.

Characterization

The morphologies of products were observed on a field emission scanning electron microscopy (FE-SEM, JEOL, JSM-7001F) and a transmission electron microscopy (TEM, JEOL, JEM-2100F). X-ray diffraction (XRD) analyses were carried out on a Philips X'Pert PRO X-ray diffractometer with a CuK_α radiation. Fourier transform infrared (FTIR) spectra with a resolution of 2 cm^{-1} were recorded on a Nicolet 6700 spectrometer (Thermo Fisher Scientific, US). The Raman spectra for the samples were obtained on a Laser Raman spectroscopy (InVia, RENISHAW) using a 514 nm argon ion laser. The electrical conductivities of the pressed pellets at room temperature were measured by a standard four-probe method on an SZ82 digital instrument. The complex permeability and permittivity of the materials were measured using a vector network analyzer (AV3618, CETC, China) in the frequency of 2 - 18 GHz. The samples were mixed with wax and prepared as the toroidal shape with an outer diameter of 7.0 mm, an inner diameter of 3.04 mm and a thickness of 4.0 mm. The mass ratios of the samples to wax were set to be 1:9.

Simulation Method

The first-principles calculations based on the density functional theory (DFT) were performed using dispersion-corrected density functional theory (DFT-D) provided by the DMol3 code.

Conclusions

In conclusion, a new approach has been put forward to efficiently synthesize graphene/PANi hybrids through an intercalation of ANi^+ into EG, which follows an *in situ* polymerization. It is found that there exist special interactions between PANi and graphene molecules, and thus, the physical parameters, say the conductivity

and permittivity in this work, of the composites display an unconventionally change compared with the pure conducting polymers or the graphene alone. The graphene/polyaniline hybrid shows significantly enhancement in microwave absorption. We reckon this kind of hybridizing structures may be a good way towards new functional design with broad adjustable parameters of graphene and its composites.

Acknowledgements

This work was financially supported by the National Natural Science Foundation of China (Nos. 51173148, 51303151, 51302230), the Science and Technology Planning Project of Sichuan Province (Nos. 2013RZ0036, 2011GZX0052), and the Fundamental Research Funds for the Central Universities of China (polymer research project).

References

1 R. S. Ruoff, *Nat. Nanotechnol.*, 2008, **3**, 10–11.
2 N. Park, S. Hong, G. Kim and S. H. Jhi, *J. Am. Chem. Soc.*, 2007, **129**, 8999–9003.
3 C. Heo, J. Yoo, S. Lee, A. Jo, S. Jung, H. Yoo, Y. H. Lee and M. Suh, *Biomaterials*, 2011, **32**, 19–27.
4 C. Wang, X. J. Han, P. Xu, X. L. Zhang, Y. C. Du, S. R. Hu, J. Y. Wang and X. H. Wang, *Appl. Phys. Lett.*, 2011, **98**, 072906–1–3.
5 F. Bonaccorso, Z. Sun, T. Hasan and A. C. Ferrari, *Nat. Photonics.*, 2010, **4**, 611–622.
6 K. S. Novoselov, A. K. Geim, S. V. Morozov, D. Jiang, Y. Zhang, S. V. Dubonos, I. V. Grigorieva and A. A. Firsov, *Science*, 2004, **306**, 666–669.
7 A. K. Geim and P. Kim, *Sci. Am.*, 2008, **298**, 90–97.
8 Y. Hernandez, V. Nicolosi, M. Lotya, F. M. Blighe, Z. Y. Sun, S. De, I. T. McGovern, B. Holland, M. Byrne, Y. K. Gun'Ko, J. J. Boland, P. Niraj, G. Duesberg, S. Krishnamurthy, R. Goodhue, J. Hutchison, V. Scardaci, A. C. Ferrari and J. N. Coleman, *Nat. Nanotechnol.*, 2008, **3**, 563–568.
9 S. F. Pei and H. M. Cheng, *CARBON*, 2012, **50**, 3210–3228.
10 T. Ohta, A. Bostwick, T. Seyller, K. Horn and E. Rotenberg, *Science*, 2006, **313**, 951–954.
11 X. S. Li, W. W. Cai, J. An, S. Kim, J. Nah, D. X. Yang, R. Piner, A. Velamakanni, I. Jung, E. Tutuc, S. K. Banerjee, L. Colombo and R. S. Ruoff, *Science*, 2009, **324**, 1312–1314.
12 J. Sun and H. Bi, *Mater. Lett.*, 2012, **81**, 48–51.
13 Y. Li, H. R. Peng, G. C. Li and K. Z. Chen, *Eur. Polym. J.*, 2012, **48**, 1406–1412.
14 Y. F. Huang and C. W. Lin, *Polymer*, 2012, **53**, 1079–1085.
15 J. Yan, T. Wei, B. Shao, Z. J. Fan, W. Z. Qian, M. L. Zhang and F. Wei, *CARBON*, 2010, **48**, 487–493.
16 S. Williams, J. R. Hummers and E. O. Richard, *J. Am. Chem. Soc.*, 1958, **80**, 1339–1339.
17 L. H. Li, X. L. Zheng, J. J. Wang, Q. Sun and Q. Xu, *ACS Sustainable Chem. Eng.*, 2013, **1**, 144–151.
18 C. Q. Liu, G. X. Hu and H. Y. Gao, *J. Supercrit. Fluids.*, 2012, **63**, 99–104.
19 V. Chabot, B. Kim, B. Sloper, C. Tzoganakis and A. P. Yu, *Sci. Rep.*, 2013, **3**, 1378–1–7.
20 J. E. Jones, M. C. Cheshire, D. J. Casadonte and C. C. Phifer, *Org. Lett.*, 2004, **6**, 1915–1917.
21 D. Krepel and O. Hod, *J. Phys. Chem. C*, 2013, **117**, 19477–19488.
22 S. Y. Jeong, S. H. Kim, J. T. Han, H. J. Jeong, S. Y. Jeong and G. W. Lee, *Adv. Funct. Mater.*, 2012, **22**, 3307–3314.
23 S. Goswami, U. N. Maiti, S. Maiti, S. Nandy, M. K. Mitra and K. K. Chattopadhyay, *CARBON*, 2011, **49**, 2245–2252.
24 K. Zhang and L. L. Zhang, *Chem. Mater.*, 2010, **22**, 1392-1401.
25 J. Stejskal, I. Sapurina, M. Trchova, E. N. Konyushenko and P. Holler, *Polymer*, 2006, **47**, 8253–8262.
26 N. A. Kumar, H. J. Choi, Y. R. Shin, D. W. Chang, L. M. Dai and J. B. Baek, *ACS NANO*, 2012, **6**, 1715–1723.
27 A. Tursun, X. G. Zhang and J. Ruxangul, *Mater. Chem. Phys.*, 2005, **90**, 367–372.
28 J. Y. Shen, C. Y. Yang, X. W. Li and G. C. Wang, *ACS Appl. Mater. Interfaces*, 2013, **5**, 8467–8476.
29 G. Q. Wang, W. Xing and S. P. Zhuo, *Electrochim. Acta.*, 2012, **66**, 151–157.
30 S. A. Chen and H. T. Lee, *Macromolecules*, 1995, **28**, 2858–2866.
31 J. Tang, X. Jing, B. Wang and F. Wang, *Synth. Met.*, 1988, **24**, 231–238.
32 M. Cochet, G. Louarn, S. Quillard, J. P. Buisson and S. Lefrant, *J Raman Spectrosc*, 2000, **31**, 1041–1049.
33 D. H. Deng, X. L. Pan, L. Yu, Y. Cui, Y. P. Jiang, J. Qi, W. X. Li, Q. Fu, X. C. Ma, Q. K. Xue, G. Q. Sun and X. H. Bao, *Chem. Mater.*, 2011, **23**, 1188–1193.
34 A. C. Ferrari, J. C. Meyer, V. Scardaci, C. Casiraghi, M. Lazzeri, F. Mauri, S. Piscanec, D. Jiang, K. S. Novoselov, S. Roth and A. K. Geim, *Phys. Rev. Lett.*, 2006, **97**, 187401–1–4.
35 V. Singh, D. Joung, L. Zhai, S. Das, S. I. Khondaker and S. Seal, *Prog. Mater. Sci.*, 2011, **56**, 1178–1271.
36 J. P. Perdew and Y. Wang, *Phys. Rev. B: Condens. Matter.*, 1992, **45**, 13244–13249.
37 J. P. Perdew, K. Burke and M. Ernzerhof, *Phys. Rev. Lett.*, 1996, **77**, 3865–3868.
38 B. Delley, *J. Chem. Phys.*, 2000, **113**, 7756–7764.
39 H. J. Monkhorst and J. D. Pack, *Phys. Rev. B*, 1976, **13**, 5188–5192.
40 S. Grimme, *J. Comput. Chem.*, 2006, **27**, 1787–1799.
41 N. R. Chiou, L. J. Lee, A. J. Epstein, *Chem. Mater.*, 2007, **19**, 3589–3591.
42 P. M. Ostrovsky, I. V. Gornyi and A. D. Mirlin, *Phys. Rev. B*, 2006, **74**, 235443–1–20.
43 H. Zengin, W. S. Zhou, J. Y. Jin, R. Czerw, D. W. Smith, L. Echegoyen, D. L. Carroll, S. H. Foulger and J. Ballato, *Adv. Mater.*, 2002, **14**, 1480–1483.
44 R. C. Che, X. F. Duan, Q. Chen, X. L. Liang, L. M. Peng, *Adv. Mater.* 2004, **16**, 401–405.
45 G. Z. Wang, Z. Gao, S. W. Tang, C. Q. Chen, F. F. Duan, S. C. Zhao, S. W. Lin, Y. H. Feng, L. Zhou, Y. Qin, *ACS NANO*, 2012, **6**, 11009–11017.
46 V. K. Singh, A. Shukla, M. K. Patra, L. Saini, R. K. Jani, S. R. Vadera, N. Kumar, *CARBON*, 2012, **50**, 2202–2208.

